Analysis of spatio temporal geophysical data using spatial entropy: application to comparison of SST datasets

Juan Gancio[1], Giulio Tirabassi[2], Cristina Masoller[1], and Marcelo Barreiro[3]

[1]Universitat Politècnica de Catalunya, Departament de Fisica, Rambla Sant Nebridi 22, Terrassa 08222, Barcelona, Spain.
[2]Universitat de Girona, Departament de Informàtica, Matemàtica Aplicada i Estadística, Universitat de Girona, Carrer de la Universitat de Girona 6, Girona 17003, Spain.
[3]Departamento de Ciencias de la atmósfera y Física de los Océanos, Facultad de Ciencias, Universidad de la República, Montevideo, 11400, Uruguay.

Correspondence: Juan Gancio (juan.gancio@upc.edu)

Abstract. Efficient data analysis techniques are urgently needed due to the large amount of data continuously generated by Earth modeling and monitoring systems. We show that the spatial permutation entropy (SPE) is a valuable technique to characterize spatio-temporal geophysical data, allowing detailed analysis at different scales. Specifically, we show that SPE is able to uncover differences in two sea surface temperature (SST) products, in two relevant geographical regions: the equatorial Pacific (Niño3.4) and the Gulf Stream. SPE is calculated as the entropy of the probabilities of occurrences of symbols that are defined along two orientations, west-east (WE) or north-south (NS), and either in consecutive grid points, or separated by a lag, δ. We find substantial differences between the analyzed datasets, for the WE orientation with $\delta = 1$, that gradually disappear as δ increases. We also identify two transitions, one in year 2007 when ERA5 changed its sea–surface boundary condition to OSTIA, and the second one in 2021 when NOAA changed satellite, from MeteOp–A to MeteOp–C. These transitions were not detected when using conventional data analysis tools, which demonstrates that SPE is a valuable tool for the analysis of 2D geophysical data.

1 Introduction

Due to the large amount of data generated by Earth modeling and monitoring systems, much effort is currently being devoted to developing new, efficient climate data analysis techniques (Messori et al., 2017; Gupta et al., 2021; Díaz et al., 2023; Krouma et al., 2024). Ordinal analysis is a symbolic method that was originally proposed for time-series analysis (Bandt and Pompe, 2002). The method is based on estimating the probabilities of symbols, known as ordinal patterns (OPs), defined in terms of the temporal order of the relative values of L data points. As an example, for $L = 3$, data values such that $x_t < x_{t+1} < x_{t+2}$ give symbol "012", values such that $x_t > x_{t+1} > x_{t+2}$ give symbol "210", values such that $x_{t+2} < x_t < x_{t+1}$ give symbol "201", etc. The symbols' probabilities are calculated and their entropy, known as permutation entropy, is a measure that detects and quantifies nonlinear temporal correlations, being low if some patterns are much more probable than others or being high if all possible patterns are equally probable. Ordinal analysis is computationally very efficient and is robust in the presence of artifacts and noise. The use of lagged (non-consecutive) data points adds versatility to the method, since it allows to select
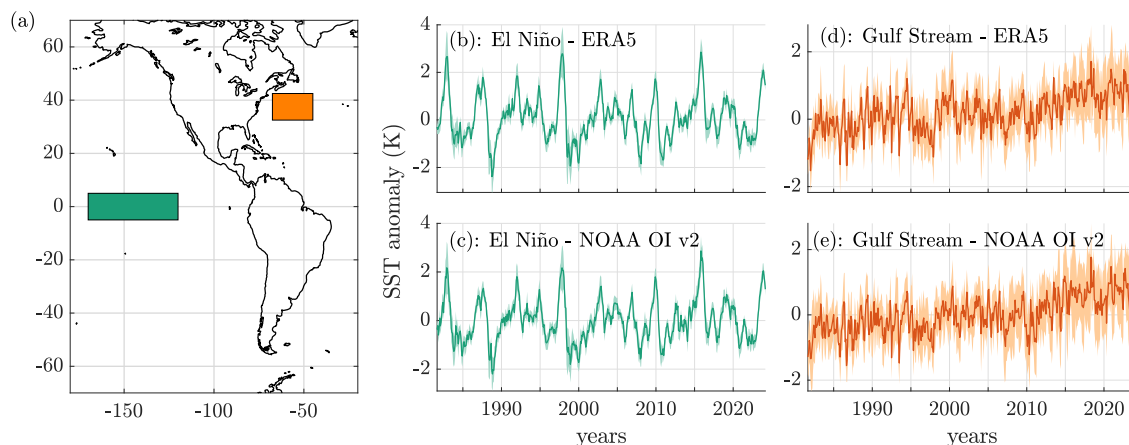
Figure 1. Panel (a) highlights the regions of interest: Niño3.4 (in green), and the Gulf Stream (in orange). Panels (b) and (c) show the SST anomaly in the Niño3.4 region, and panels (d) and (e), in the Gulf Stream region, calculated from ERA5 (b, d) and NOAA OI v2 (c, e) datasets. In panels (b)–(e), the thick lines represent the spatial mean of the anomalies, while the shading indicates the spatial standard deviation.

different temporal scales for the analysis. By applying ordinal analysis to time-series of surface air temperature anomalies, long-range tele-connections with different time-scales have been detected (Barreiro et al., 2011; Deza et al., 2013).

25 Ordinal analysis can be applied to two-dimensional spatial data, by defining the OPs in terms of the spatial order of the relative values of L data points. Spatial ordinal analysis is a versatile tool because one can chose different "shapes" for the symbols. For example, for symbols with $L = 4$ data points one can consider the relative values of 2×2 points, a line of 4 points, an "L" composed by $3 + 1$ points, etc. Furthermore, the use of spatially lagged data points allows to select the spatial scale of the analysis.

30 The spatial permutation entropy (SPE) has been used to analyze images, art works and textures (Ribeiro et al., 2012; Sigaki et al., 2018, 2019; Tirabassi and Masoller, 2023; Tirabassi et al., 2023; Muñoz-Guillermo, 2023). It has also been used to analyze biomedical data such as EEG recordings (Boaretto et al., 2023; Gancio et al., 2024) and cardiac synthetic data (Schlemmer et al., 2015, 2018). However, to our knowledge, SPE has not yet been tested on climate data.

Since SPE can be calculated from the relative values of a climate variable at a given time in a particular geographic region,
35 it can yield information about the nonlinear spatial correlations of that variable at that time, in that region. In contrast, the "temporal" permutation entropy of the variable at a particular grid point is calculated by considering segments of the time series and computing the ordinal probabilities in each segment.

Our goal is to demonstrate that SPE a reliable and versatile tool. We focus on a key variable, sea surface temperature (SST), and compare two SST products in two key regions, the equatorial Pacific and the the Gulf Stream. We show that SPE identifies
40 differences in the datasets in short spatial scales, which can be more or less pronounced in different periods of time. We interpret our findings in terms of the methodologies and data used to construct the SST products.

2 Data

We consider monthly SST anomalies in El Niño3.4 region (170W–120W, 5N–5S), and in the western north Atlantic (32.5N–42.5N, 67.5W–45W), a box centered on the Gulf Stream (see Fig. 1a). We analyze NOAA Optimal Interpolation version 2

45 (Reynolds et al., 2007; Huang et al., 2021), and ERA5 global reanalysis (Hersbach et al., 2020). Both datasets have spatial resolution of $0.25^o \times 0.25^o$. ERA5 starts in January 1940, while NOAA starts in September 1981; both extend to March 2024. See Appendix A for additional information about the data.

3 Ordinal patterns and spatial permutation entropy

In the ordinal approach, the values of SST anomalies in L grid points at a given time are represented by an ordinal pattern (OP)

50 that is assigned according to the spatial ordering of relative SST values (see Appendix B and Fig. B1). There are $L!$ possible patterns and from their probabilities, p_j, the spatial permutation entropy is calculated

$$H = -\frac{1}{\log(L!)} \sum_{j=1}^{L!} p_j \log(p_j).$$ (1)

H is close to 1 when there is no spatial order in the data (all OPs are equally likely), and is < 1 if the data presents gradients that make some OPs more/less probable. Since SST values vary over time, H is a function of time.

55 The method is versatile because a particular spatial orientation can be used for selecting L grid points, and they can be neighboring points or not (see Sec. B2 and Fig. B1b). In the next section we consider linear sets of $L = 4$ grid points with north-south (NS) or west-east (WE) orientation with spatial lag δ (for $\delta = 1$ the points are consecutive grid points). H_{WE} (H_{NS}) represents SPE calculated using grid points aligned in WE (NS) direction respectively.

4 Results

60 Figure 2 displays the results for $\delta = 1$, for the two datasets, in the two analyzed regions. In Niño3.4 region, we observe a large difference in H_{WE} values until 2007. Then, the differences are small until 2022, when the values start diverging again. These periods coincide with the switch of the sea-surface boundary condition of ERA5, from HadISST2 to OSTIA, in 2007 (Hersbach et al., 2020), and the inclusion of MeteOp-C satellite data in NOAA's dataset in November 2021 (Jonasson et al., 2020), respectively. We can also observe that H_{WE} variance for the NOAA data remains stationary through the time span,

65 while for ERA5, H_{WE} variance increases with time. This effect is also present in H_{NS}, although to a lesser extent, and, overall, the H_{NS} variation in the two datasets agree.

Differences are also observed for the Gulf Stream region; they are more pronounced in H_{NS} and become small in 2013. This could be due to the update of the background error covariances on OSTIA in January 2013 (Good et al., 2020; Roberts-Jones et al., 2016). We also observe differences between H_{WE} values starting around 2018, which could be due to the fact

70 that OSTIA underwent several updates around this time, including an upgrade to feature resolution using NEMOVAR (Fiedler
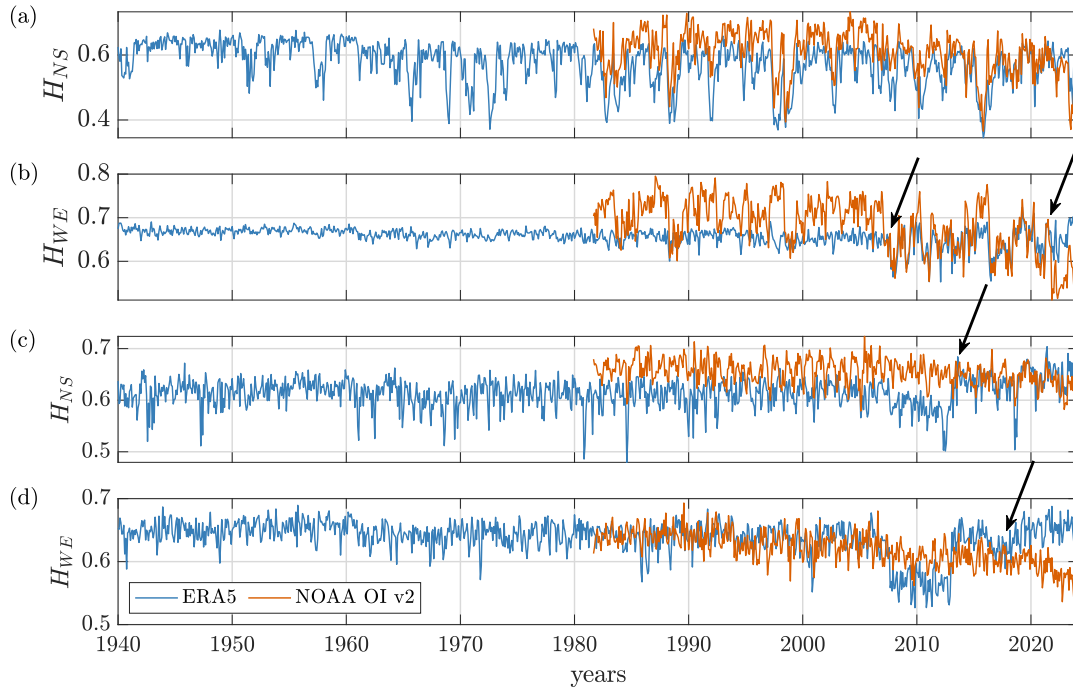
Figure 2. Entropies calculated with spatial lag $\delta = 1$ in (a),(b) Niño3.4 region; (c),(d) Gulf Stream region. Arrows indicate the changes-transitions discussed in the text.

et al., 2019), the addition of infrared data from Sentinel-3A SLSTR (Good et al., 2020), and the inclusion of MetOp-C AVHRR data.

Figure 3 displays the results obtained when the grid points are spaced by a lag $\delta = 8$ (2°). In this case, both datasets agree well, in the two regions and for the two OP orientations because the variation of H_{WE} and H_{NS} in ERA5 and in NOAA is consistent. In Nino3.4 region, H_{WE} has a negative trend, which can be due to SST variation over the equatorial Pacific, since it warms in the west and cools in the east (Wills et al., 2022), which means there is a westward large-scale gradient over the Niño3.4 area that can make symbols that represent trends more prevalent, decreasing the entropy (that is maximum when all possible symbols are equally probable).

From 1981 (when NOAA dataset starts) sudden H_{WE} drops are observed, which tend to correlate to El Niño/La Niña events and can be interpreted as due to the spatial structures formed by the uneven warming/cooling of the region during these events, which accentuate due to global warming (Cai et al., 2014; Xie et al., 2010); however, H_{WE} also decreases during other periods and further analysis is needed to understand the mechanisms underlying these variations.

In the Gulf Stream region, which is also heating due to global warming (Seidov et al., 2017; Todd and Ren, 2023), H_{WE} and H_{NS} in ERA5 and in NOAA present a positive trend, which reveals a loss of spatial structure (as the different symbols become more equally probable), and this fact is consistent with the homogeneous heating of this region.
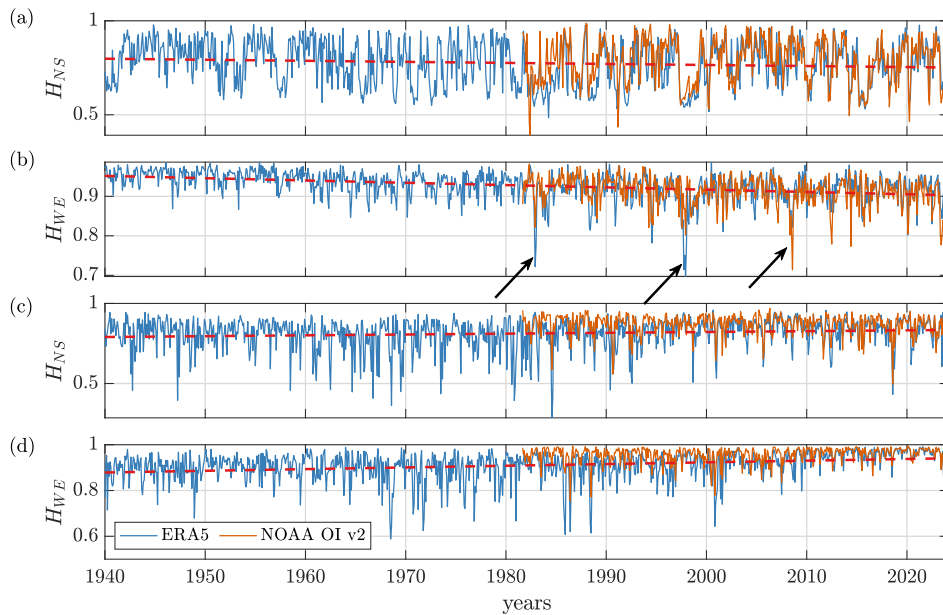
Figure 3. Entropies calculated with $\delta = 8$ in (a),(b) Niño3.4 region; (c),(d) Gulf Stream region. Dashed lines indicate linear fittings of the ERA5 data; the arrows indicate large variations discussed in the text.

Figure 4 displays H_{NS} and H_{WE} for different lags between the grid points. To more clearly display similarities and differences between ERA5 and in NOAA, we only analyze the period when both datasets are available (1981–2024). We observe that as δ increases the behavior of H_{NS} and H_{WE} for the two datasets converge, which indicates that the differences found between ERA5 and NOAA occur mainly at short spatial scales.

90 Finally, to demonstrate the added value of using nonlinear ordinal analysis, we present the results obtained with two well-known measures of linear relationship between two datasets: the average absolute difference, AAD, and the spatial Pearson's correlation coefficient, r.

They provide complementary information because when AAD and r are both high, the datasets differ in values but their spatial distributions are consistent, whereas when both are low, there is agreement between the values, but not in the spatial

95 distributions (see definitions on Appendix C). In Fig. 5 we see that both measures show continuous improvement of the agreement between the two datasets in the two regions, however, there are oscillations and no clear transitions are observed. In the Gulf Stream region AAD and r show a strong coupling with the annual cycle, with disagreement (high AAD and low r) peaking during northern winters. Increased cloud coverage in this region during winters could difficult infrared measurements, which may lead to larger differences between ERA5 and NOAA datasets. On the other hand, in Niño3.4 region ENSO events

100 affect the agreement between the datasets, but their effect is captured differently by the two measures. For example, AAD
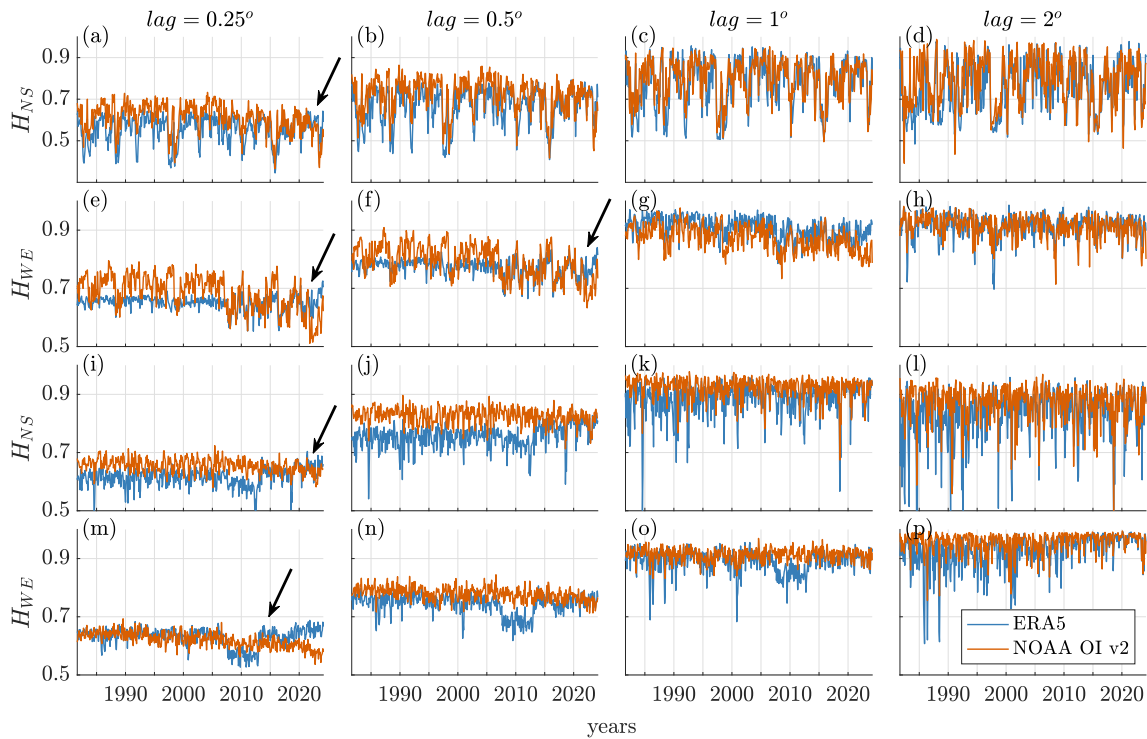
Figure 4. Effect of the lag between grid points. Panels (a)–(h) correspond to the Niño3.4 region, and (i)–(p) to the Gulf Stream region. Arrows indicate when the tendency that ERA5 provides lower entropy values reverses.

peaks during El Niño in 1988, 1997 and during La Niña of 2011, but these events do not affect r, and vice-versa, La Niña in 1996 and 1999, and El Niño in 2004, affect r but not AAD.

Regarding the transition in 2007 detected with ordinal analysis, only in r we observe a period of high values starting in 2007, although the transition to this state not as sharp as the one uncovered by SPE. In both regions we observe a later period when
105 r returns back to similar values as before 2007 (2011–2015 for Niño3.4, and 2012–2016 for Gulf Stream), after which both stabilize to values very close to 1 (see Appendix C2 for further analysis using the mutual information). No clear transition is observed in 2021 in r, nor in AAD.

5 Conclusions

We have used a nonlinear quantifier, the spatial permutation entropy, SPE, to analyze ERA5 and NOAA OI v2 SST anomalies
110 in two key regions of the world, Niño3.4 and Gulf Stream. We calculated the temporal variation of SPE over several decades using symbols that were defined in terms of four values of SST anomalies, geographically oriented either north-south (NS) or west-east (WE), which were taken as neighboring grid points, or spatially separated by a lag.
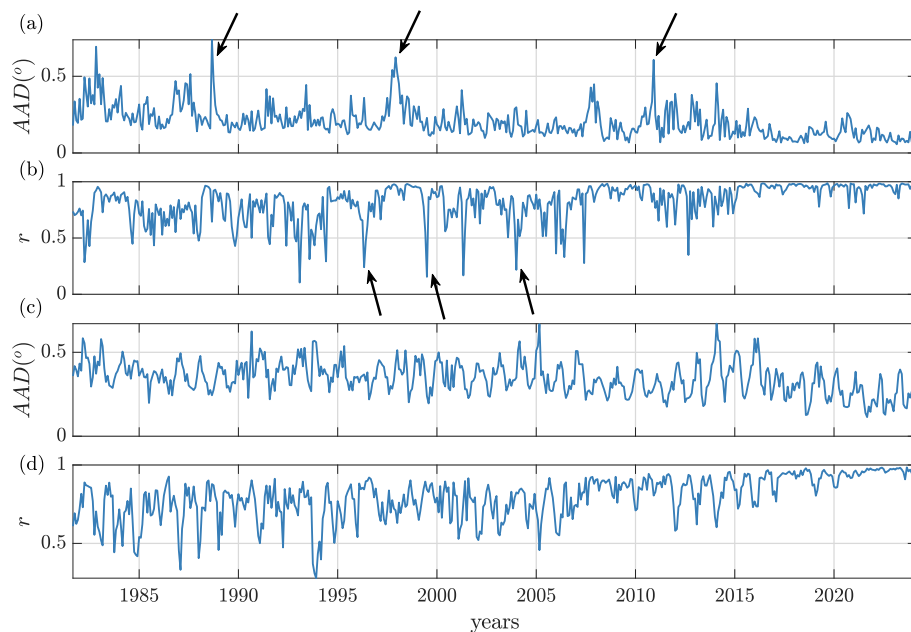
Figure 5. Average absolute difference, AAD, and spatial Pearson's correlation coefficient, r, between ERA5 and NOAA datasets in (a), (b) Niño3.4 region, and (c), (d) Gulf Stream region. Arrows indicate ENSO events discussed in the text.

We found differences between the two datasets in short spatial scales but these differences disappear as the spatial scale of the analysis increases. The SPE temporal variation allowed us to identify two particular transitions, the first one in 2007, which corresponds to the year when ERA5 changed its sea-surface boundary condition to OSTIA and the second one in 2021, which corresponds to the year when NOAA SST changed satellite, from MeteOp-A to MeteOp-C. These differences add on to previously reported discrepancies (Yao et al., 2021; Dai, 2023). Moreover, the different SPE trends found on the equatorial Pacific and Gulf Stream regions in the last decades are consistent with different responses to greenhouse gas forcing (uneven warming/cooling and homogeneous heating respectively).

Taken together, our results show that SPE is a flexible quantifier to analyze the spatio-temporal dynamics of a climatological variable. We have shown that SPE detects well-defined transitions in the analyzed datasets, which have a physical interpretation, while linear measures reveal continuous variations with oscillations but no clear changes.

For future work, it will be interesting to explore the spatio-temporal permutation entropy proposed by Schlemmer et al. (2018), which integrates in the definition of the OPs the spatial and temporal variation of a climatological variable. It could also be interesting to perform the analysis when the OPs integrate information using different temporal lags (Barreiro et al., 2011), or from different climatological variables, for example, defining OPs from the values of surface air temperature and SST anomalies in each grid point. In addition, training machine learning algorithms with features obtained with ordinal analysis (that

encapsulate new information) might allow to improve the forecasts of state-of-the-art climate models, in particular, regarding large-scale phenomena that have stochastic periodicity, such as ENSO.

130 *Code and data availability.* NOAA OI v2 data was obtained from the KNMI Climate Explorer (https://climexp.knmi.nl/select.cgi?id=someone@somewhere&field=sstoiv2_monthly_mean). ERA5 data was obtained from the Copernicus Climate Data Store (https://cds.climate.copernicus.eu/datasets/reanalysis-era5-single-levels-monthly-means?tab=overview). The code used for the analysis and the generation of the figures is available at https://github.com/juangancio/climate-spatial-analysis, and archived at https://doi.org/10.5281/zenodo.14055559.

Appendix A: Data

135 NOAA SST includes observations from ships, drifting and moored buoys, and the Advanced Very High Resolution Radiometer (AVHRR) (Huang et al., 2021) retrieved from NOAA series and MetOp-A/-B satellites by U.S Navy before November 2021. After this date, NOAA SST switched to the Advanced Clear Sky Processor for Ocean (ACSPO) (Huang et al., 2023; Jonasson et al., 2020) satellite SSTs retrieved from AVHRR and the Visible Infrared Imager Radiometer Suite (VIIRS) (Huang et al., 2023).

140 ERA5 SST is the combination of HadISST2 (Titchner and Rayner, 2014) up to August 2007 and OSTIA (Donlon et al., 2012) from September 2007 onwards (Hirahara et al., 2016). HadISST2 assimilates in-situ observations as well as two radiometers: AVHRR and the Along Track Scanning Radiometer (ATSR).

OSTIA was originally constructed at a resolution of 0.05^o and includes in situ data from various sources, as well as derived from several satellite products including AVHRR and VIIRS. It is worth noting that the higher resolution of OSTIA allows it 145 to better resolve the tropical instability waves and sub-mesoscale eddies in the midlatitudes (Hirahara et al., 2016).

Within the regions of interest, both datasets provide us with similar grids (with 40×200 grid points for the Niño3.4, and 40×90 for the Gulf Stream region), the only difference being a small offset of 0.005^o both in latitude and longitude.

Appendix B: Spatial permutation entropy

B1 Ordinal patterns

150 Ordinal analysis is a nonlinear data analysis technique proposed by Bandt and Pompe (2002), that has been extensively applied for more than 20 years in a wide variety of different scientific fields. This technique takes an ordered series of values that represents the evolution of a certain variable (usually known as time series), x_i, where $x_t \in \mathbb{R}$, and $t \in [1, \dots, N]$, and translates it into a sequence of symbols: s_t. This operation requires only two parameters: the word length, L, and a delay, δ. These parameters are used to select a sequence of L data points $[x_t,\ x_{t+\delta},\ x_{t+2\delta},\ \dots,\ x_{t+(L-1)\delta}]$, which is assigned the symbol 155 $s_t = [\pi(t),\ \pi(t+\delta),\ \dots,\ \pi(t+(L-1)\delta)]$ where $\pi(\cdot)$ is the permutation index that sorts the selection in ascending order: $x_{\pi(t)} \le x_{\pi(t+\delta)} \le \cdots \le x_{\pi(t+(L-1)\delta)}$. As an example, if the ordinal patterns are defined in terms of three consecutive data
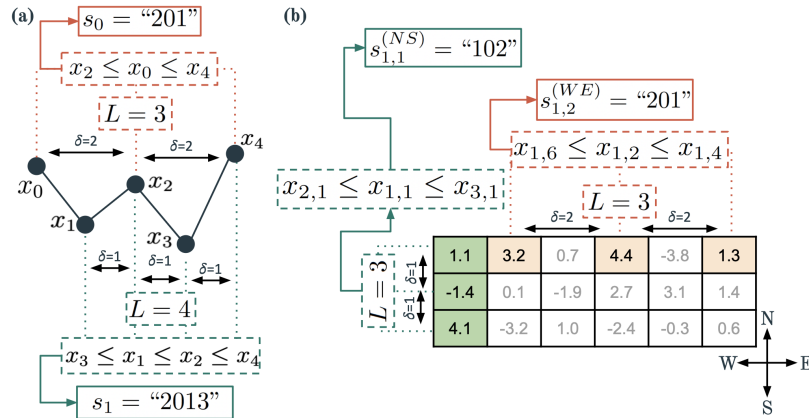
Figure B1. Procedure to obtain the different ordinal patterns (OP). Panel (a) shows the usual approach to obtain OP from a 1-dimensional time series (with examples of two combinations of parameters $L = 3$ and $\delta = 2$, and $L = 4$ and $\delta = 1$. Panel (b) shows the proposed approach to obtain symbols with NS and WS orientation from the 2D datasets (examples with $L = 3$ and $\delta = 2$, and $L = 3$ and $\delta = 2$).

points, the number of possible patterns is $L! = 6$ and the data points $(3.2, 4.4, 1.3)$ give pattern "201", while $(1.3, 3.2, 4.4)$ gives pattern "012" and $(4.4, 3.2, 1.3)$ pattern "210". This operation is repeated for every $t = 1, \ldots, n = N - (L-1)\delta$, producing a n–length sequence of the possible $L!$. If n_i is the number of times that the symbol i appears in this new sequence, then the

160   probability of the symbol is $p_i = n_i/n$, with $i \in [1, \ldots, L!]$. This probability distribution is then used to calculate the Shannon entropy (Eq. 1), know as permutation entropy.

B2   Symbol orientations in 2D spatio-temporal data

We now consider the time evolution of a 2-dimensional $N \times M$ gridded set of data, $X_{i,j}(t)$, $i \in [1, \ldots, N]$, $j \in [1, \ldots, M]$, $t = 1, \ldots, T$, such as index i corresponds to different latitudes, and index j to different longitudes, and T the number of time

165   steps in the series. Given the parameters L (word length), and δ (spatial lag), we construct two sets of symbols: those with WE alignment ($\{X_{i,j}(t), X_{i,j+\delta}(t), \ldots, X_{i,j+\delta(L-1)}(t)\} \forall i \in [1, \ldots, N]$ and $j \in [1, \ldots, M - \delta(L-1)]$), and those with NS alignment ($\{X_{i,j}(t), X_{i+\delta,j}(t), \ldots, X_{i+\delta(L-1),j}(t)\} \forall i \in [1, \ldots, N - \delta(L-1)]$ and $j \in [1, \ldots, M]$). Observe that unless $N = M$, these set of symbols have different number of elements, n: $n = (N - \delta(L-1))M$ for WE symbols, and $n = N(M - \delta(L-1))$ for NS ones. From the probabilities of these symbols we can straightwardly calculate the permutation entropies for each

170   time step t, $H_{WE}(t)$ and $H_{NS}(t)$, using Eq. 1.

Appendix C: Quantitative comparisons between the datasets

In order to quantify the agreement between both datasets, we have calculated different linear and non-linear measures of their spatial coherence. If we write the two datasets as the time evolution of 2D arrays: $X_{i,j}(t)$ and $Y_{i,j}(t)$ (it does not matter which array represents which datasets, since all the measures here presented are symmetric); we introduce the following measures.
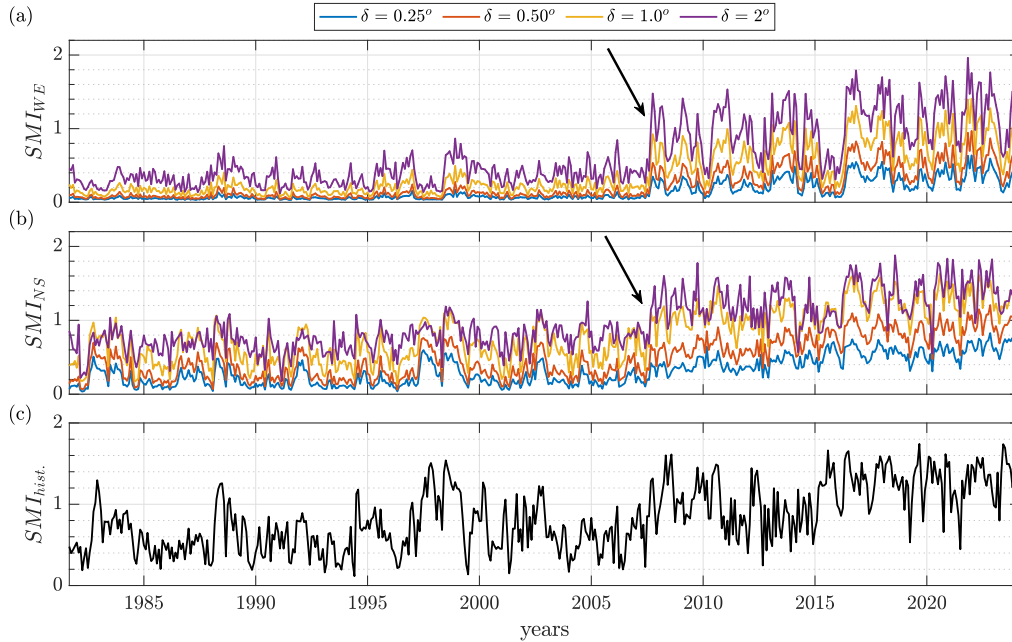
Figure C1. Spatial mutual information for the Niño3.4 region. In panel (a) the probabilities are obtained from ordinal patterns (OP) of WE orientation, $L = 4$ and different spatial lags (δ), idem for panel (b) but for OP with NS orientation; in panel (c) the probabilities are obtained from the histograms of values ($bins = 24$). Arrows indicate the transition observed in 2007.

C1 Linear quantities

Average absolute difference (AAD):

$$AAD(t) = \langle |X_{i,j}(t) - Y_{i,j}(t)| \rangle_{i,j}.$$

Pearson's spatial correlation coefficient (r):

$$r(t) = \frac{\sigma_{X,Y}(t)}{\sigma_X(t)\sigma_Y(t)},$$

where $\sigma_X(t)$ and $\sigma_Y(t)$ represent the spatial variances of the datasets at time t, and $\sigma_{X,Y}(t)$ their spatial covariance at time t. Both quantities are reported in Fig. 5.

C2 Non linear quantities – Spatial mutual information

Similarly as we obtained the spatial entropies from both datasets (Eq. 1), $H_X(t)$ and $H_Y(t)$, we can estimate the probability of same-position occurrence (an spatial analogue of simultaneous occurrence in the time domain) from which the joint spatial entropy can be calculated:

$$H_{X,Y}(t) = -\sum_{i,j}^{L!} p_{i,j}(t) \log(p_{i,j}(t)).$$
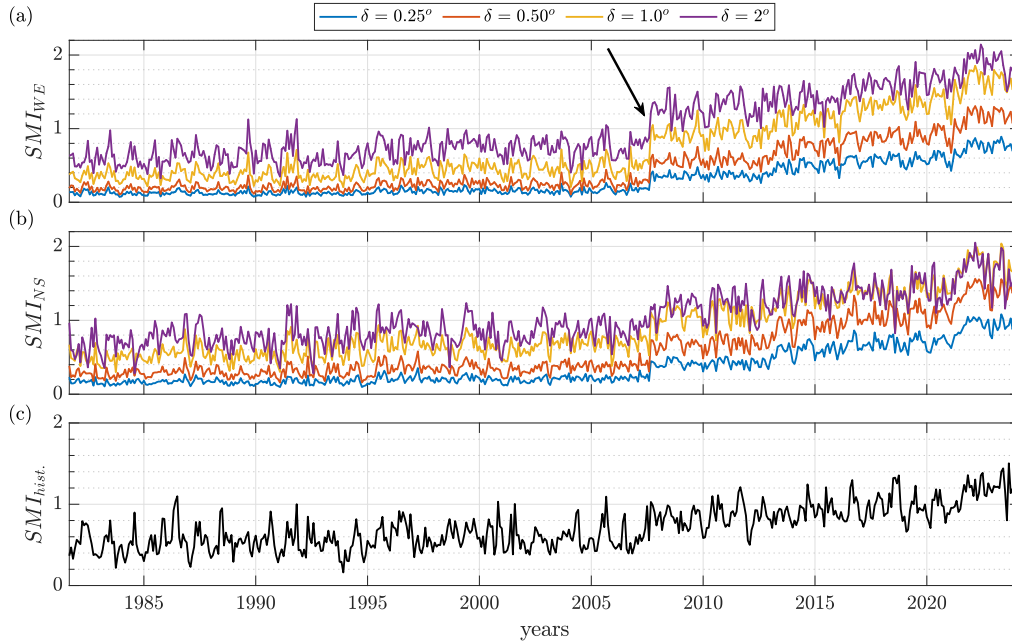
Figure C2. Same as Fig. C1 but for the Gulf Stream region.

From these three quantities we can calculate the spatial mutual information (SMI) (Celik, 2016; Kumar and Bhandari, 2022):

$$SMI(t) = H_X(t) + H_Y(t) - H_{X,Y}(t).$$

Depending on what probabilities distributions are used to obtain the entropies, different values of SMI can be computed. We
180 have considered the probabilities coming from histogram of values (SMI_{hist}), and from OP symbols (SPE) with North-South
(SMI_{NS}) and West-East orientation (SMI_{WE}), which are shown in Figs. C1 and C2, respectively. In all cases the probabilities
distributions consist in 24 possible values (bins), corresponding to $L = 4$ in the OP approach. For the SPE approach, we can
see how SMI increases with δ, for all regions and orientations. For the NS orientation, it is also observed in both regions that
$\delta = 1^o$ and $\delta = 2^o$ produce similar outputs, suggesting that all small scale difficulties in this orientation are already resolved at
185 the 1° scale.

For el Niño3.4 region (Fig. C1), SMI_{NS} and SMI_{WE} both reveal a clear transition at the end of 2007, which is more clear
on the bigger scales. We stress the importance of such results, since it is the SMI which provides the first indication of this
transition at the larger scales, something that our initial assessment missed (Figs. 3 and 4). In addition, before 2007 SMI_{WE}
present exceptionally low values, which also accentuate the transition in this variable. After 2007, both oscillate around a
190 certain constant value, with a little increase on 2016. We note that SMI_{WE} seems to be strongly coupled with the warm phase
of ENSO, which greatly impact in the coherence between the datasets, as we can observe during the ElNiño events of 1997,
2010, and 2015, to name a few. We highlight that this effect is observed at all scales, and in the current configuration of the

datasets, since it is observed during the 2023 warm ENSO event. Regarding $SMI_{hist.}$, it is observed some increase in the average value around 2007 and 2015, but the transitions seems to be softer than for the other SMI values reported.

195   For the Gulf Stream region (Fig. C2), all three SMI values reported present oscillations around a relative constant value before 2007, which seems to start to increase consistently from this year on. Again, this transition is the most evident on SMI_{WE}. We observe that the annual cycle has some an impact on $SMI_{hist.}$, but not on SMI_{NS}, nor SMI_{WE}.

Author contributions. JG: conceptualization, formal analysis, methodology, software, writing – original draft, writing – review & editing. GT: conceptualization, software, supervision, writing – original draft, writing – review & editing. CM: conceptualization, supervision, writing

200   – original draft, writing – review & editing. MB: supervision, writing – original draft, writing – review & editing.

Competing interests. The authors declare that they have no conflict of interest.

Acknowledgements. We acknowledge the support of ICREA ACADEMIA, AGAUR (2021 SGR 00606 and FI scholarship), and Ministerio de Ciencia e Innovación (Project No. PID2021-123994NB-C21).

References

205 Bandt, C. and Pompe, B.: Permutation entropy: a natural complexity measure for time series, Physical review letters, 88, 174 102, 2002.

Barreiro, M., Marti, A. C., and Masoller, C.: Inferring long memory processes in the climate network via ordinal pattern analysis, Chaos, 21, 013 101, 2011.

Boaretto, B. R., Budzinski, R. C., Rossi, K. L., Masoller, C., and Macau, E. E.: Spatial permutation entropy distinguishes resting brain states, Chaos, Solitons & Fractals, 171, 113 453, 2023.

210 Cai, W., Borlace, S., Lengaigne, M., Van Rensch, P., Collins, M., Vecchi, G., Timmermann, A., Santoso, A., McPhaden, M. J., Wu, L., et al.: Increasing frequency of extreme El Niño events due to greenhouse warming, Nature climate change, 4, 111–116, 2014.

Celik, T.: Spatial mutual information and PageRank-based contrast enhancement and quality-aware relative contrast measure, IEEE Transactions on Image Processing, 25, 4719–4728, 2016.

Dai, A.: The diurnal cycle from observations and ERA5 in surface pressure, temperature, humidity, and winds, Climate Dynamics, 61,
215 2965–2990, 2023.

Deza, J. I., Barreiro, M., and Masoller, C.: Inferring interdependencies in climate networks constructed at inter-annual, intra-season and longer time scales, Eur. Phys. J. Special Topics, 222, 511–523, 2013.

Díaz, N., Barreiro, M., and Rubido, N.: Data driven models of the Madden-Julian Oscillation: understanding its evolution and ENSO modulation, npj Climate and Atmospheric Science, 6, 203, 2023.

220 Donlon, C. J., Martin, M., Stark, J., Roberts-Jones, J., Fiedler, E., and Wimmer, W.: The operational sea surface temperature and sea ice analysis (OSTIA) system, Remote Sensing of Environment, 116, 140–158, 2012.

Fiedler, E., Mao, C., Good, S., Waters, J., and Martin, M.: Improvements to feature resolution in the OSTIA sea surface temperature analysis using the NEMOVAR assimilation scheme, Quarterly Journal of the Royal Meteorological Society, 145, 3609–3625, 2019.

Gancio, J., Masoller, C., and Tirabassi, G.: Permutation entropy analysis of EEG signals for distinguishing eyes-open and eyes-closed brain
225 states: Comparison of different approaches, Chaos, 34, 043 130, 2024.

Good, S., Fiedler, E., Mao, C., Martin, M. J., Maycock, A., Reid, R., Roberts-Jones, J., Searle, T., Waters, J., While, J., et al.: The current configuration of the OSTIA system for operational production of foundation sea surface temperature and ice concentration analyses, Remote Sensing, 12, 720, 2020.

Gupta, S., Boers, N., Pappenberger, F., and Kurths, J.: Complex network approach for detecting tropical cyclones, Climate Dynamics, 57,
230 3355–3364, 2021.

Hersbach, H., Bell, B., Berrisford, P., Hirahara, S., Horányi, A., Muñoz-Sabater, J., Nicolas, J., Peubey, C., Radu, R., Schepers, D., et al.: The ERA5 global reanalysis, Quarterly Journal of the Royal Meteorological Society, 146, 1999–2049, 2020.

Hirahara, S., Balmaseda, M. A., Boisseson, E., and Hersbach, H.: 26 sea surface temperature and sea ice concentration for ERA5, Eur. Centre Medium Range Weather Forecasts, Berkshire, UK, ERA Rep. Ser, 26, 2016.

235 Huang, B., Liu, C., Banzon, V., Freeman, E., Graham, G., Hankins, B., Smith, T., and Zhang, H.-M.: Improvements of the daily optimum interpolation sea surface temperature (DOISST) version 2.1, Journal of Climate, 34, 2923–2939, 2021.

Huang, B., Yin, X., Carton, J. A., Chen, L., Graham, G., Liu, C., Smith, T., and Zhang, H.-M.: Understanding differences in sea surface temperature intercomparisons, Journal of Atmospheric and Oceanic Technology, 40, 455–473, 2023.

Jonasson, O., Gladkova, I., Ignatov, A., and Kihai, Y.: Progress with development of global gridded super-collated SST products from low
240 Earth orbiting satellites (L3S-LEO) at NOAA, in: Ocean Sensing and Monitoring XII, vol. 11420, pp. 5–22, SPIE, 2020.

Krouma, M., Specq, D., Magnusson, L., Ardilouze, C., Batté, L., and Yiou, P.: Improving subseasonal forecast of precipitation in Europe by combining a stochastic weather generator with dynamical models, Quarterly Journal of the Royal Meteorological Society, 2024.

Kumar, R. and Bhandari, A. K.: Spatial mutual information based detail preserving magnetic resonance image enhancement, Computers in Biology and Medicine, 146, 105 644, 2022.

245 Messori, G., Caballero, R., and Faranda, D.: A dynamical systems approach to studying midlatitude weather extremes, Geophysical Research Letters, 44, 3346–3354, 2017.

Muñoz-Guillermo, M.: Multiscale two-dimensional permutation entropy to analyze encrypted images, Chaos, 33, 013 112, 2023.

Reynolds, R. W., Smith, T. M., Liu, C., Chelton, D. B., Casey, K. S., and Schlax, M. G.: Daily high-resolution-blended analyses for sea surface temperature, Journal of climate, 20, 5473–5496, 2007.

250 Ribeiro, H. V., Zunino, L., Lenzi, E. K., Santoro, P. A., and Mendes, R. S.: Complexity-entropy causality plane as a complexity measure for two-dimensional patterns, PLoS One, 7, e40 689, 2012.

Roberts-Jones, J., Bovis, K., Martin, M. J., and McLaren, A.: Estimating background error covariance parameters and assessing their impact in the OSTIA system, Remote Sensing of Environment, 176, 117–138, 2016.

Schlemmer, A., Berg, S., Shajahan, T., Luther, S., and Parlitz, U.: Quantifying spatiotemporal complexity of cardiac dynamics using ordinal
255 patterns, in: 2015 37th Annual International Conference of the IEEE Engineering in Medicine and Biology Society (EMBC), pp. 4049–4052, IEEE, 2015.

Schlemmer, A., Berg, S., Lilienkamp, T., Luther, S., and Parlitz, U.: Spatiotemporal Permutation Entropy as a Measure for Complexity of Cardiac Arrhythmia, Front. in Phys., 6, 39, 2018.

Seidov, D., Mishonov, A., Reagan, J., and Parsons, R.: Multidecadal variability and climate shift in the North Atlantic Ocean, Geophysical
260 Research Letters, 44, 4985–4993, 2017.

Sigaki, H. Y. D., Perc, M., and Ribeiro, H. V.: History of art paintings through the lens of entropy and complexity, PNAS, 115, E8585–E8594, 2018.

Sigaki, H. Y. D., de Souza, R. F., de Souza, R. T., Zola, R. S., and Ribeiro, H. V.: Estimating physical properties from liquid crystal textures via machine learning and complexity-entropy methods, Phys. Rev. E, 99, 013 311, 2019.

265 Tirabassi, G. and Masoller, C.: Entropy-based early detection of critical transitions in spatial vegetation fields, PNAS, 120, e2215667 120, 2023.

Tirabassi, G., Duque-Gijon, M., Tiana-Alsina, J., and Masoller, C.: Permutation entropy-based characterization of speckle patterns generated by semiconductor laser light, APL Photonics, 8, 126 112, 2023.

Titchner, H. A. and Rayner, N. A.: The Met Office Hadley Centre sea ice and sea surface temperature data set, version 2: 1. Sea ice
270 concentrations, Journal of Geophysical Research: Atmospheres, 119, 2864–2889, 2014.

Todd, R. E. and Ren, A. S.: Warming and lateral shift of the Gulf Stream from in situ observations since 2001, Nature Climate Change, 13, 1348–1352, 2023.

Wills, R. C., Dong, Y., Proistosecu, C., Armour, K. C., and Battisti, D. S.: Systematic climate model biases in the large-scale patterns of recent sea-surface temperature and sea-level pressure change, Geophysical Research Letters, 49, e2022GL100 011, 2022.

275 Xie, S.-P., Deser, C., Vecchi, G. A., Ma, J., Teng, H., and Wittenberg, A. T.: Global warming pattern formation: Sea surface temperature and rainfall, Journal of Climate, 23, 966–986, 2010.

Yao, L., Lu, J., Xia, X., Jing, W., and Liu, Y.: Evaluation of the ERA5 sea surface temperature around the Pacific and the Atlantic, IEEE Access, 9, 12 067–12 073, 2021.